RESEARCH ARTICLE | JULY 05 2023

Resistance transient dynamics in switchable perovskite memristors

Juan Bisquert ; Agustín Bou ; Antonio Guerrero ; Enrique Hernández-Balaguera

APL Mach. Learn. 1, 036101 (2023)
https://doi.org/10.1063/5.0153289

Resistance transient dynamics in switchable perovskite memristors

Cite as: APL Mach. Learn. 1, 036101 (2023); doi: 10.1063/5.0153289
Submitted: 6 April 2023 • Accepted: 23 May 2023 •
Published Online: 5 July 2023

Juan Bisquert,[1,a)] Agustín Bou,[1] Antonio Guerrero,[1] and Enrique Hernández-Balaguera[2]

AFFILIATIONS

[1] Institute of Advanced Materials (INAM), Universitat Jaume I, 12006 Castelló, Spain
[2] Escuela Superior de Ciencias Experimentales y Tecnología (ESCET), Universidad Rey Juan Carlos, 28933 Móstoles, Madrid, Spain

[a)] **Author to whom correspondence should be addressed:** bisquert@uji.es

ABSTRACT

Memristor devices have been investigated for their properties of resistive modulation that can be used in data storage and brain-like computation elements as artificial synapses and neurons. Memristors are characterized by an onset of high current values under applied voltage that produces a transition to a low resistance state or successively to different stable states of increasing conductivity that implement synaptic weights. Here, we develop a nonlinear model to explain the variation with time of the voltage and the resistance and compare it to experimental results on ionic–electronic halide perovskite memristors. We find separate experimental signatures of the capacitive discharge and inductive current increase. We show that the capacitor produces an increase step of the resistance due to the influence of the series resistance. In contrast, the inductor feature associated with inverted hysteresis causes a decrease of the resistance, as observed experimentally. The chemical inductor feature dominates the potentiation effect in which the conductivity increases with the voltage stimulus. Our results enable a quantitative characterization of highly nonlinear electronic devices using a combination of techniques such as time transient decays and impedance spectroscopy.

I. INTRODUCTION

The continuous development of artificial intelligence powered by neural networks, which can receive physical inputs from a wide range of sensors, has paved the way for the creation of various applications capable of performing numerous automated tasks. For instance, autonomous vehicles utilize various sensors, such as cameras, radars, and lidars, to perceive their environment and make decisions accordingly. In the healthcare industry, wearable devices can track vital signs and provide alerts in the case of abnormal readings. Similarly, in the manufacturing sector, machines equipped with sensors can detect anomalies in the production process and take corrective measures automatically.

However, there is a concern that the expansion of artificial intelligence for improved efficiency and productivity across various industries is accompanied by a significant amount of energy consumption. Accordingly, new computational systems that mimic the natural brain are being developed.[1] Well suited for perception, cognition, and motor tasks, these methods are adaptive, fault-tolerant, and scalable and process information using energy-efficient, asynchronous, and event-driven techniques. One candidate for the development of brain-like neuromorphic systems is the memristor element that can be formed in several material platforms for the functions of synapses and neurons.[2–9] Memristors are highly nonlinear systems that show resistive switching under voltage cycling.[10,11] One type of system shows an abrupt jump to a low resistance state where an ohmic response is observed at high voltages.[12,13] These are useful as volatile memories and only show two states of current: the highly resistive state during the sweep in the forward direction of the I–V curve and the low resistive state in the backward direction. On the other hand, to use a memristor as a synapse, it is necessary to program it with distinct non-volatile resistive states that can support spike timing-dependent plasticity, as shown in Fig. 1.[10,14–17]

By construction, memristors show intense hysteresis and memory effects that have been the topic of current investigations especially for the multistate memristors for synaptical functions.[17,18] One central property of a memristor is the temporal evolution of the resistance that is described in Fig. 2 for a halide perovskite $CsPbBr_3$

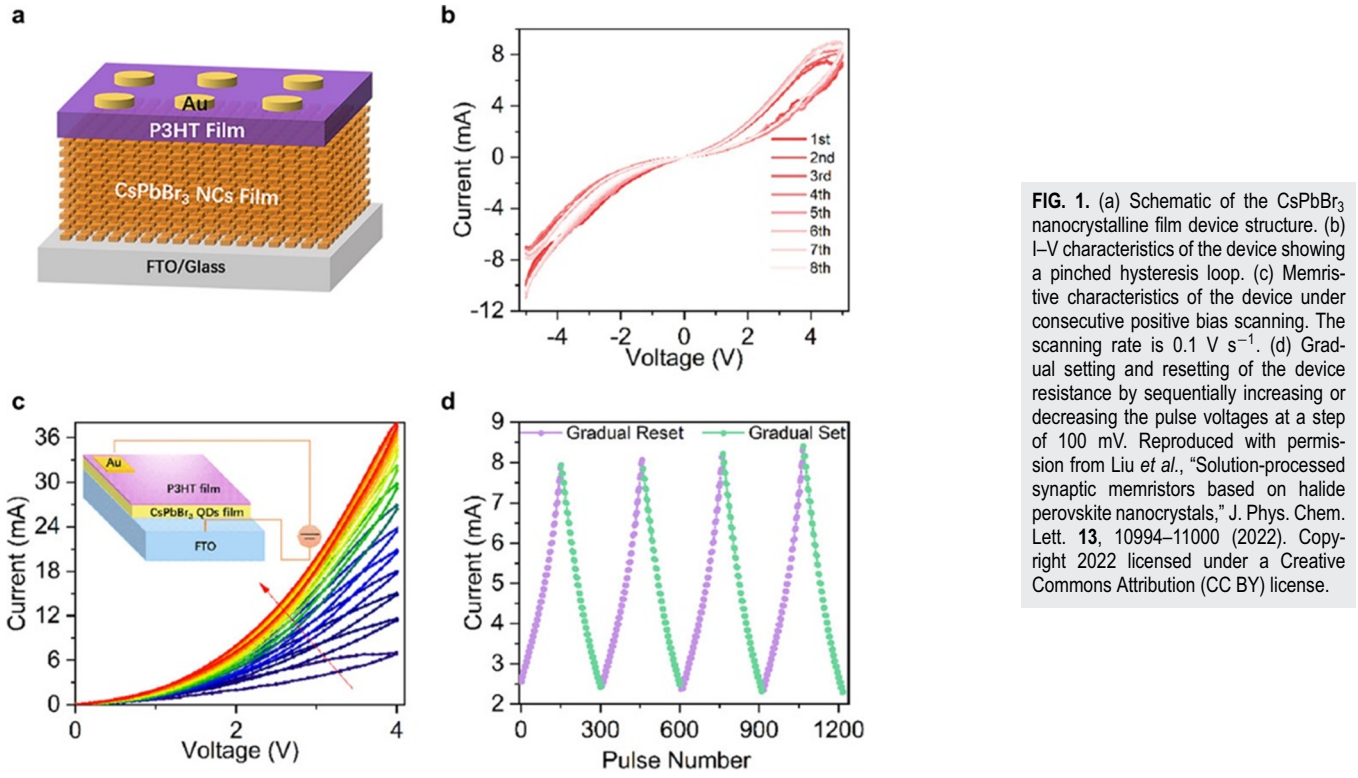

FIG. 1. (a) Schematic of the $CsPbBr_3$ nanocrystalline film device structure. (b) I–V characteristics of the device showing a pinched hysteresis loop. (c) Memristive characteristics of the device under consecutive positive bias scanning. The scanning rate is 0.1 V s^{-1}. (d) Gradual setting and resetting of the device resistance by sequentially increasing or decreasing the pulse voltages at a step of 100 mV. Reproduced with permission from Liu *et al.*, "Solution-processed synaptic memristors based on halide perovskite nanocrystals," J. Phys. Chem. Lett. **13**, 10994–11000 (2022). Copyright 2022 licensed under a Creative Commons Attribution (CC BY) license.

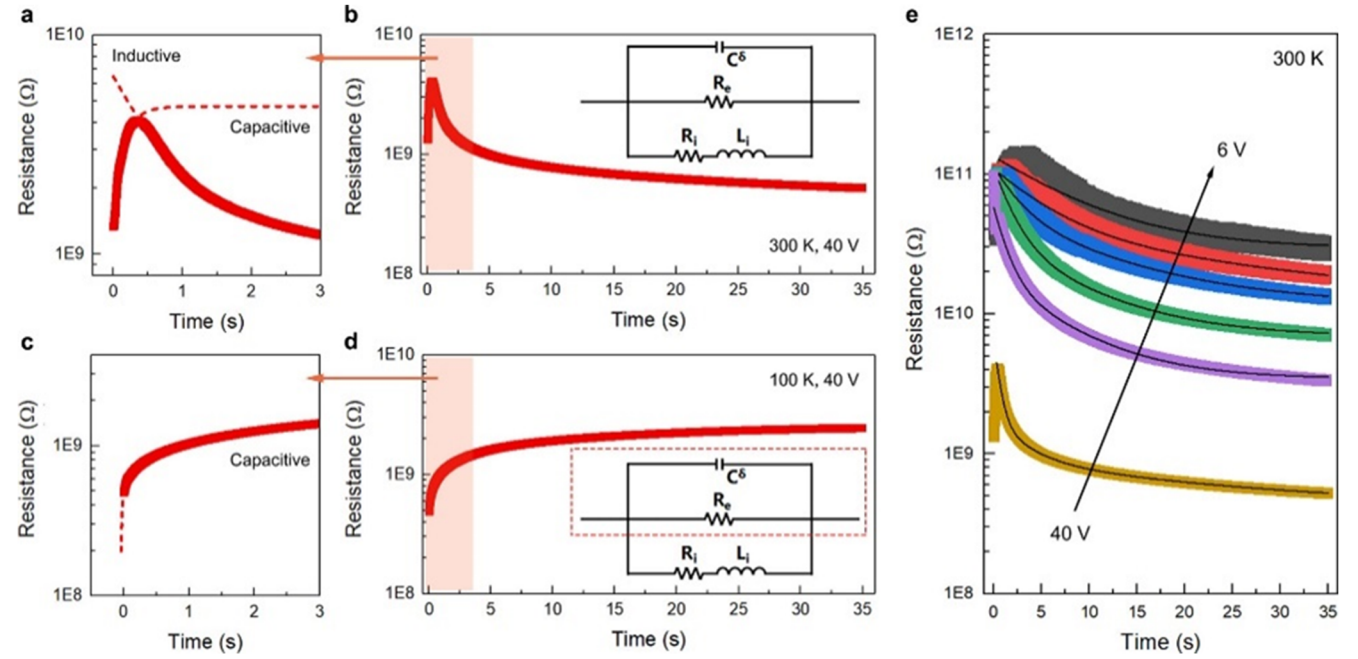

FIG. 2. Resistance of a $CsPbBr_3$ nanocrystalline film extracted from the potentiostatic measurements at (a) and (b) room temperature (300 K) and (c) and (d) low temperature (100 K). The dashed lines in (a) and (c) represent exponential fittings of the slow ionic inductive component and the fast trap-related capacitive component, respectively. Insets of (b) and (d) show the equivalent circuit. (e) Voltage-dependent resistance of the $CsPbBr_3$ nanocrystalline film extracted from the potentiostatic measurements at room temperature. The black solid lines represent exponential fittings of the slow ionic inductive component under different voltages. Reproduced with permission from Liu *et al.*, "Solution-processed synaptic memristors based on halide perovskite nanocrystals," J. Phys. Chem. Lett. **13**, 10994–11000 (2022). Copyright 2022 licensed under a Creative Commons Attribution (CC BY) license.

nanocrystalline film device.[9] The experimental results show the dominant effect of a chemical inductor[19,20] in the temporal response of the memristor. In this paper, we apply a recently developed nonlinear memristor model[21–23] for a quantitative description and interpretation of the current transients and the peaks of memristor resistance under voltage pulses.

II. THE MEMRISTOR MODEL

We describe the memristor by the dynamical equations of the total current I_{tot} with respect to the applied voltage V_{app},[21]

$$V_{app} = R_s I_{tot} + u, \tag{1}$$

$$I_{tot} = C_m \frac{du}{dt} + \frac{u}{R_b} + i_c, \tag{2}$$

$$\tau_k \frac{di_c}{dt} = \frac{i_{c0}}{1 + e^{-(u-V_T)/V_m}} - i_c. \tag{3}$$

Here, R_s is a series resistance and u is the voltage in the active layer of the device. The model is nonlinear and cannot be represented as a linear circuit; hence, we use the scheme of Fig. 3(a). The current I_{tot} has three components: a capacitive charging with capacitance C_m, an ohmic current of constant resistance R_b (the intrinsic high resistance of the system), and the slow internal current described by the variable i_c, which produces the transition to the high conduction state. As explained before,[21] Eq. (3) represents a diffusion or reaction time of ions[18,24] that introduces a delay of i_c with respect to the external perturbation by the characteristic time constant τ_k. In the steady state, the slow current has the sigmoidal form,

$$i_c = i_{c0} f_{ss}(u), \tag{4}$$

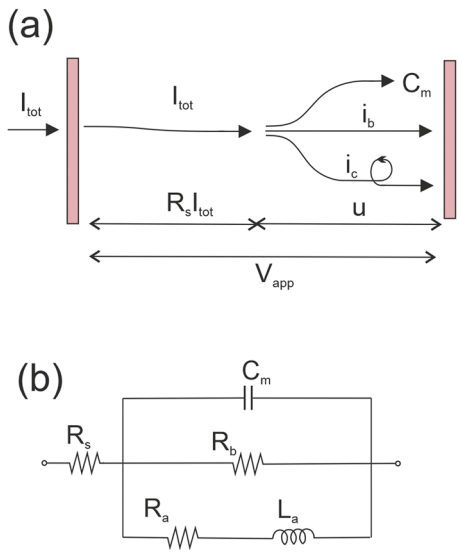

FIG. 3. (a) Scheme of the dynamical model showing total current I_{tot} and voltage V_{app}, internal voltage u, and conduction (i_b, i_c) and capacitive (C_m) currents between the current collector plates. (b) Corresponding equivalent circuit model for small signal ac perturbation in impedance spectroscopy.

$$f_{ss} = \frac{1}{1 + e^{-(u-V_T)/V_m}}. \tag{5}$$

Thus, i_c varies from 0 at low voltage to a saturation value i_{c0} at high voltage, with the activation potential V_T and an ideality factor V_m with dimension of voltage. The physical mechanisms governing the change of f_{ss} are the filamentary conductive pathway[6,25] or the decrease of a surface barrier between the perovskite layer and the contacts.[26,27]

The steady state current and voltage shown in Figs. 4(a) and 4(b) (gray line) is described by the following equation, where u_{app} is obtained from Eq. (1):

$$I_{dc} = \frac{u_{app}}{R_b} + \frac{1}{1 + e^{-(u_{app}-V_T)/V_m}} i_{c0}. \tag{6}$$

III. AC IMPEDANCE PROPERTIES

By linearization of Eqs. (1)–(3) at a steady-state point, the impedance spectroscopy response function in terms of the variable $s = i\omega$ can be obtained, where ω is the angular frequency of the small perturbation. The impedance function is[22,23]

$$Z(s) = R_s + \left[C_m s + {R_b}^{-1} + \frac{1}{R_a + L_a s} \right]^{-1}, \tag{7}$$

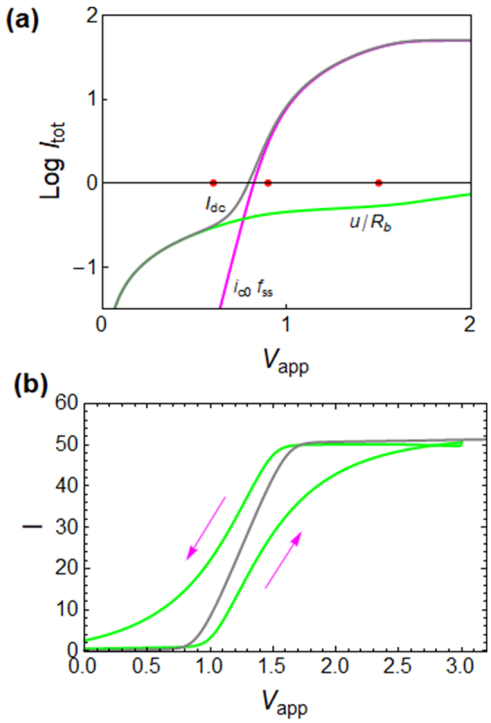

FIG. 4. (a) Logarithmic current–voltage curve for the model memristor, showing the two component currents and the total equilibrium dc current (gray line). The red points indicate the voltages at which the impedance response is analyzed. (b) The gray line is the equilibrium current–voltage curve, and the green lines are the current when the external voltage is cycled at a constant scan rate $b_s = 0.05$. Parameters $R_s = 0.01$, $R_b = 2$, $C_m = 10$, $\tau_k = 10$, $i_{c0} = 50$, $V_T = 1$, and $V_m = 0.05$.

$$R_a^{-1} = \frac{di_c}{du} = \frac{i_{c0}}{V_m} f_{ss}(1 - f_{ss}), \tag{8}$$

$$L_a = \tau_k R_a. \tag{9}$$

The model of Eq. (7) is the recently described impedance of a chemical inductor.[19] It is characteristically observed in halide perovskite devices in the high voltage domain.[28,29] The equivalent circuit is shown in Fig. 3(b), and the impedance parameters are represented in Fig. 5(a). These elements are changing by orders of magnitude under the application of voltage corresponding to the highly nonlinear nature of the system.

The interpretation of the equivalent circuit (EC) elements of Fig. 3(b) is as follows. C_m is a capacitance element as already mentioned. In halide perovskites, the large low frequency capacitance is of ionic nature.[21,29,30] The elements resistance R_a and inductor L_a are the components of the chemical inductor branch in the equivalent circuit. These elements are formed by the delay equation [Eq. (3)],[19] which in the case of halide perovskites is interpreted as an electronic current that depends on ionic displacement.[21,31] In the model, the memristor is characterized by an increase of current, Fig. 4, and a decrease of resistance, Fig. 5(a), due to the activation of the chemical inductor line of Fig. 3(b) (decrease of R_a) when the voltage approaches the threshold value V_T. The dc resistance is

$$R_{dc} = R_s + \left[R_b^{-1} + R_a^{-1}\right]^{-1}. \tag{10}$$

In the following, we explore the interplay of capacitance and inductance in synaptic memristors based on the nonlinear neuron-style model developed in perovskite solar cells, Eqs. (1)–(3).[20,32] Capacitive transients have been already described for semiconductor LEDs,[33] and the potentiation of synapses was explained based on the same model.[34]

The connection between the impedance features and hysteresis properties under voltage scan has been elucidated in halide perovskites[32,35] and related areas.[36] In capacitive hysteresis, the

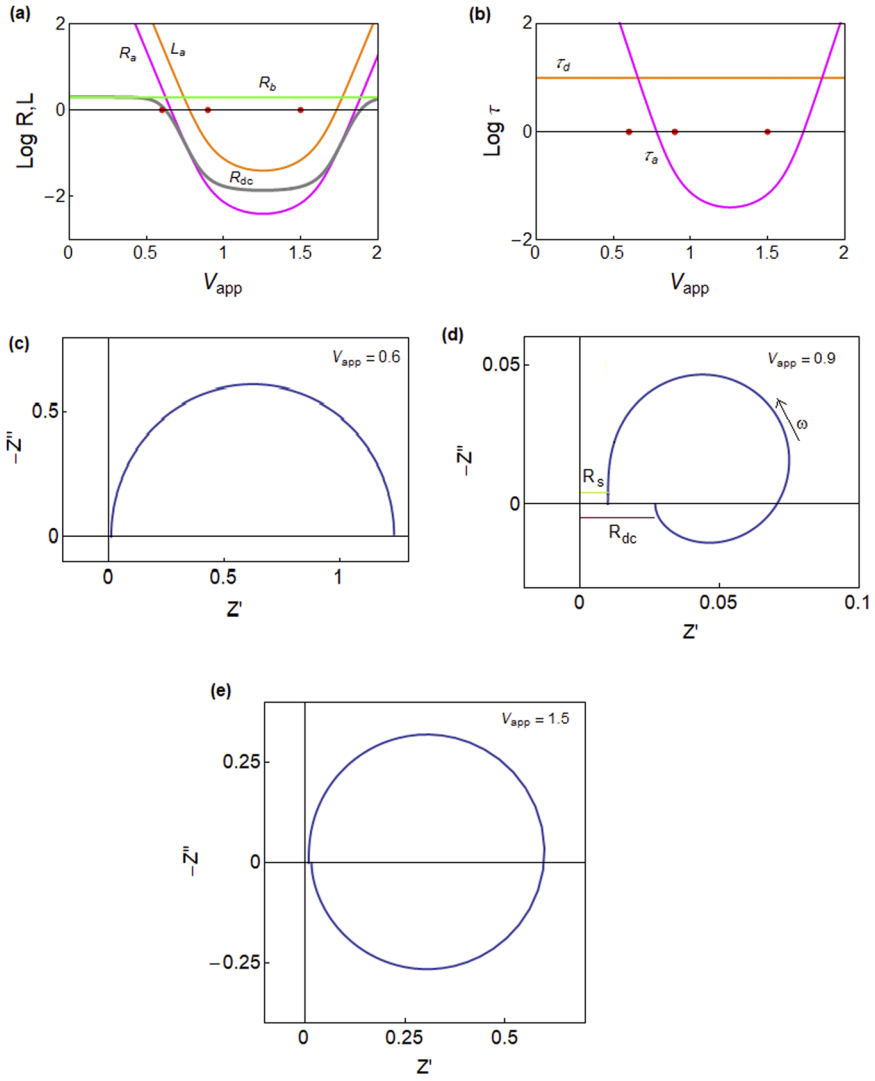

FIG. 5. (a) Equivalent circuit parameter dependence of applied voltage parameters. (b) Time constants. The red points indicate the voltages at which impedance response is shown. (c)–(e) Impedance spectra at the indicated applied voltages. Parameters $i_{c0} = 50$, $V_T = 1$, $V_m = 0.05$, $R_s = 0.01$, $R_b = 2$, $C_m = 10$, and $\tau_k = 10$.

current increases at a higher scan rate. However, when the low frequency impedance is dominated by a chemical inductor, the current decreases at a higher scan rate and the inverted hysteresis pattern of Fig. 1(b), which is a frequent characteristic of memristors, is obtained. Figure 4(b) shows the result of continuously cycling the applied voltage in the model of Eqs. (1)–(3) at a constant scan rate b_s. The current–voltage curves are characterized by inverted hysteresis due to the effect of the inductor.[32,37]

Let us consider the characteristic impedance spectra. At low applied voltage, the impedance spectra are fully capacitive, Fig. 5(c). As in Fig. 5(a), the inductor L_a is activated at a certain bias voltage. Therefore, as shown in Figs. 5(d) and 5(e), at higher voltage, the inductive feature is developed in the fourth quadrant of the complex impedance plane. For a quantitative control of this change, let us define the time constants

$$\tau_a = R_a C_m, \tag{11}$$

$$\tau_d = \frac{L_a}{R_a}. \tag{12}$$

In this case the inductor time constant equals the kinetic parameter τ_k. It can be shown[19] that the crossing to the fourth quadrant occurs when the condition

$$\tau_d > \tau_a \tag{13}$$

is satisfied. The crossing of the time constants that marks the appearance of the inductive feature is shown in Fig. 5(b). Another significant time constant for the charging of the capacitor is

$$\tau_s = R_s C_m. \tag{14}$$

IV. TIME TRANSIENT RESPONSE

The current response of a perovskite memristor to a voltage step pulse to the value V_{app} can be understood from the equivalent circuit. The best way for explaining this response is to separate it into different moments, as indicated in Fig. 6(a).

The very first moment corresponds to the high frequency part of the impedance spectrum. At this point, the parallel capacitance is shorted, and therefore, the parallel resistances R_b and R_a have no current going through them. The total resistance of the system is reduced only to the series resistance R_s. Accordingly, the memristor will initially take the current value corresponding to the gray line, $\Delta I = V_{app}/R_s$, point A, which corresponds to the minimum value of impedance, as in the spectrum of Fig. 5(d).

Immediately after, the capacitance gets charged. Then, the current starts decreasing by the time constant τ_s, until the value of the ac resistance is maximum, point B. This can be clearly seen through the impedance spectrum: at intermediate frequencies, the spectrum crosses the real axis at the maximum value of the resistance. If the time constant of the R–L branch τ_d is large enough, the inductor will take a long time to charge and will initially behave as an open circuit; therefore, the total resistance of the system at this intermediate step will be close to $R_s + R_b$ (green line), i.e., all the current goes through R_b. The current response will follow its minimum value, point B; see Fig. 6(b).

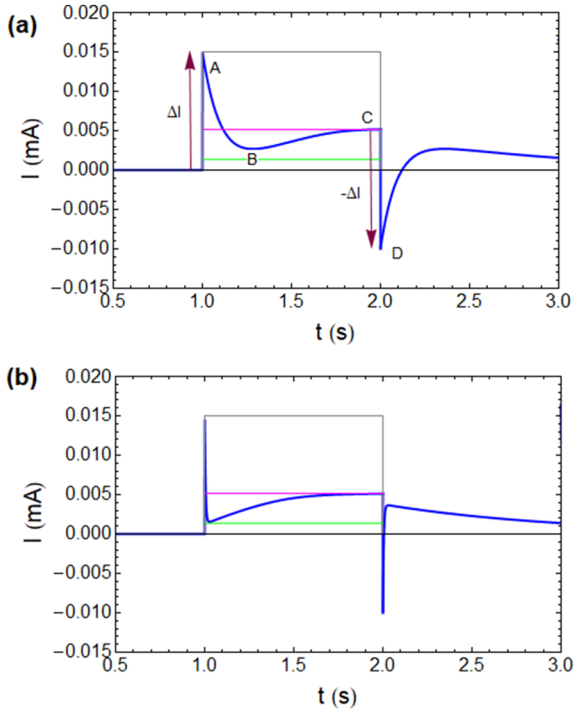

FIG. 6. (a) Transient charging current for the memristor model for a square voltage pulse $V_{app} = 1.5$. Parameters $R_b = 10^3$; $R_s = 100$; $C_m = 10^{-3}$, $i_{c0} = 10^{-2}$; $V_T = 1$; $V_m = 0.05$; $\tau_k = 1$; $\tau_s = 0.1$. The gray line is $\Delta I = V_{app}/R_s$, the magenta line is V_{app}/R_{dc}, and the green line is $V_{app}/(R_s + R_b)$. (b) Transient for $C_m = 0.05 \times 10^{-3}$, $\tau_s = 0.005$.

When time reaches the order τ_d, the inductor starts passing current. The essential property of the inductor is that once the capacitor has already been fully charged, the current still increases with time, as shown in Fig. 6(a).[20] These effects are well known in solid-state electronics.[38–41] When it is completely activated, the current reaches the magenta line, point C. Here, the inductor behaves as a short circuit and the total ac resistance of the system decreases from its maximum point. Looking at the impedance spectrum, at lower frequencies, the impedance decreases from the maximum resistance to a lower value through the arc of the fourth quadrant, Fig. 5(d). At zero frequency, the impedance gets the R_{dc} value, which is the series resistance R_s plus the resulting resistance of parallel R_b and R_a, Eq. (10).

Finally, we observe the inversion of the current when the voltage is set to 0. If the internal voltage at the moment of switch off is u_f, the voltage in the resistance must be $-u_f = I_{tot}R_s$. Hence, the negative current increment is the same as the initial step, point D.

To sum up, we have described transient patterns that are well observed in the potentiation of perovskite synapses.[5] In applying a step, we have a maximum at the very first moment, when the total resistance is only the series resistance. Then, the current decreases to its minimum, when the resistance maximizes due to the slow response of the inductor. Finally, the inductor permits the flow of current and the total resistance reduces. At this point, the current

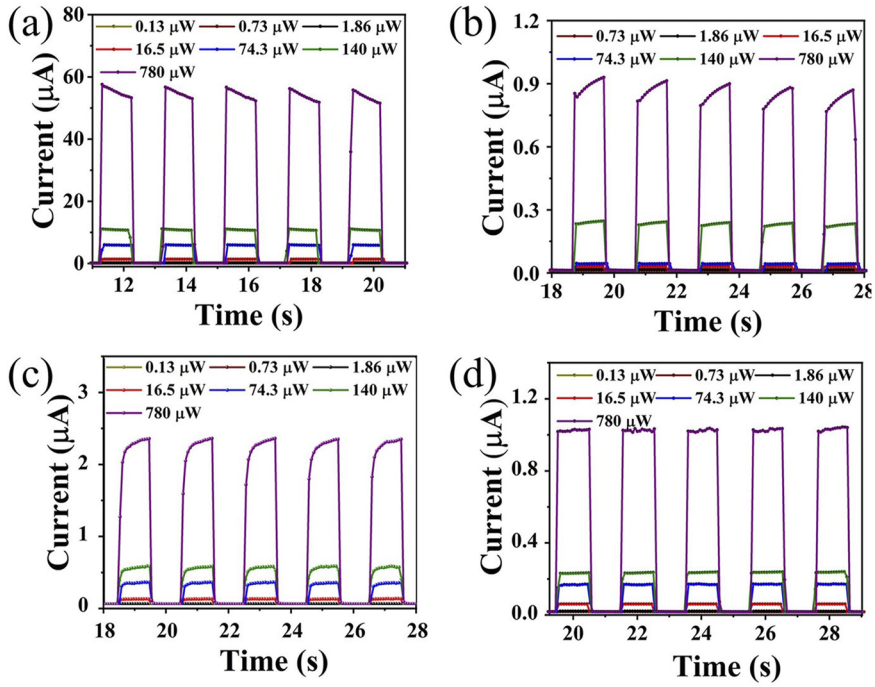

FIG. 7. Photoresponse of four mixed halide perovskite single crystal photodetectors. The illumination power varied from 0.13 to 780 μW. Reprinted with permission from Ding *et al.*, "Unraveling the effect of halogen ion substitution on the noise of perovskite single crystal photodetector," J. Phys. Chem. Lett. **13**, 7831–7837 (2022). Copyright 2022 American Chemical Society.

gradually increases to its steady-state value. A negative current is observed upon disconnecting the voltage.[33] These patterns consisting of slow charging features due to a chemical inductor property can be observed in the transient behavior of different types of devices, as in photoswitching experiments in light detectors and photoelectrochemical cells.[42,43] In Fig. 7, the feature is shown for halide perovskite photodetectors.[42] It is observed that the current rises after the initial spike in cases (b) and (c), while (a) and (d) show a different type of response.

We have described here a single charge–discharge cycle. In the potentiation of synapses over multiple steps, the system remembers the voltage of the previous cycle[5,42,44–49] and the current increases gradually, as shown in Fig. 1(c). We conclude that the chemical inductor is an essential feature for the gradual rise of the synaptic conductivity.[18,24] These properties have been recently explained elsewhere.[34]

V. RESISTANCE TRANSIENTS

We next analyze the transients of the total resistance as those shown in Fig. 2. Results are obtained by integrating Eqs. (1)–(3), as shown in Fig. 8. In (a), we apply a low voltage in which the inductor feature is negligible. The transient current shown in Fig. 8(a) is fully capacitive as discussed in Fig. 6(a). The resistance shown in Fig. 8(b) is calculated as V_{app}/I. This resistance makes a transition from the initial value R_s to the final value given by

$$R_f = \frac{V_{\rm app}}{I_{dc}}. \tag{15}$$

We conclude that in the capacitive transient, the resistance increases. Note that $R_f > R_{dc}$ with respect to the small perturbation value R_f indicated by the magenta line, Eq. (10).

When the applied voltage pulse is larger in Figs. 8(c) and 8(d), the inductor is stimulated. The small parallel resistance R_a is activated, and the total resistance decreases in the inductive domain, as shown in Fig. 8(d). Overall, there is a peak shape in the resistance vs time: the rising capacitive part and the decreasing inductive part. These features are, indeed, reported in Fig. 2[9] and in the supplementary material of Ref. 5.

The previous analysis in Figs. 8(b)–8(d) shows that the resistance measured as instantaneous V/I is, in general, different from the small ac perturbation resistance, that is, the low frequency value of the impedance, obtained as $R_{dc} = Z(\omega = 0)$, Eq. (10). The use of V/I is convenient for transient measurement, as it is well defined at any moment. In contrast to this, ac impedance gives more general information, but it needs to be measured at stationary points. This is not feasible, in general, as the memristor has an internal dynamics of the state variable x that cannot be controlled externally. Therefore, it is not warranted that one can measure the full ac impedance up to very low frequency unless the I–V curve can be stabilized, as explained elsewhere.[50]

For the sake of the analysis, let us assume that $Z(\omega)$ can be obtained in a wide frequency range while the step voltage is applied. Then, one can define the instantaneous total ac resistance as

$$R_{tot}(t) = R_s + \left[R_b^{-1} + R_a(t)^{-1}\right]^{-1}. \tag{16}$$

The calculation of the current and resistance response is shown in Fig. 9 for the same decays as in Fig. 8. In Fig. 9(a), we observe that the charging of the capacitor by the voltage step activates R_a and produces the stepping down of the total dc resistance toward the equilibrium value R_{dc}. When the applied voltage pulse is larger, the inductor is stimulated. As a consequence, in Fig. 9(b), after the capacitive decrease of the resistance, another feature appears in

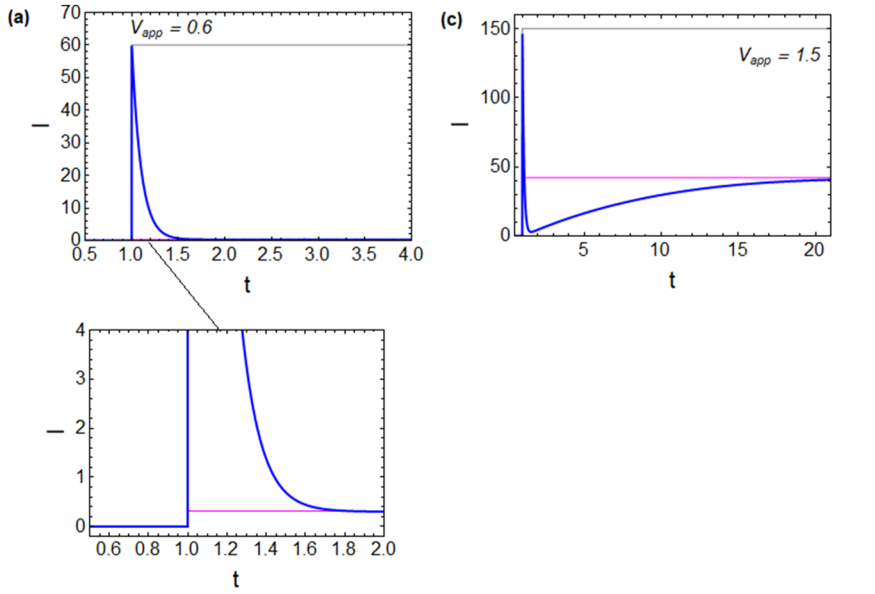

FIG. 8. Time transient response of current (I) and total resistance (R) to a voltage step V_{app} in the memristor model. (a) and (b) $V_{app} = 0.6$. (c) and (d) $V_{app} = 1.5$. The gray line in the current graphs is the initial target value V_{app}/R_s when all the voltage is at the series resistance. The magenta line is the steady state value of the current and the low frequency ac impedance value. Parameters $i_{c0} = 50$, $V_T = 1$, $V_m = 0.05$, $R_s = 0.01$, $R_b = 2$, $C_m = 10$, and $\tau_k = 10$.

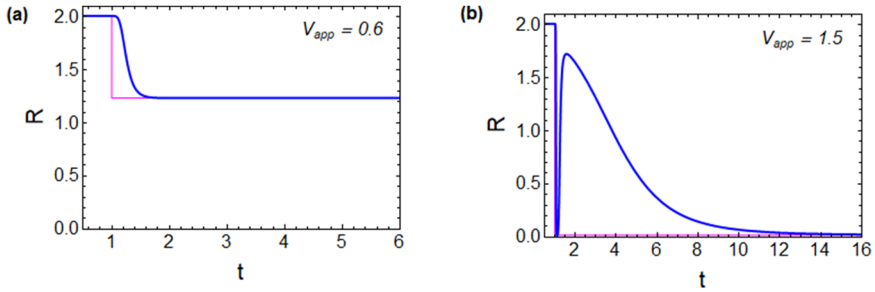

FIG. 9. Small perturbation resistance values during a voltage step V_{app} in the memristor model; same transient currents as in Fig. 5. The magenta line is the steady state value. Parameters $i_{c0} = 50$, $V_T = 1$, $V_m = 0.05$, $R_s = 0.01$, $R_b = 2$, $C_m = 10$, and $\tau_k = 10$.

which it increases and then decreases with time. Therefore, it must be remarked that the ac measurements should be made once the system is stabilized, and the impedance value is constant with time.

VI. GENERAL SIGNIFICANCE

The model of Eqs. (2) and (3) can be generalized as follows:

$$I_{tot} = C_m \frac{du}{dt} + f(u,x), \tag{17}$$

$$\tau_k \frac{dx}{dt} = g(u,x). \tag{18}$$

Here, f is a conductivity function, and the changes of the "slow" state variable x are controlled by a driven adaptation function $g(u,x)$ with the characteristic time τ_k. The above system of equations corresponds to the general structure of a voltage-controlled memristor,[51] where impedance and stability properties have been recently described.[19,23,52,53] For any combinations of configurational functions $[f(u,x), g(u,x)]$, the equivalent circuit in Fig. 3(b) is obtained in every case. Hence, the transient properties discussed in Sec. IV can be obtained in very different circumstances.

However, there are different possibilities according to the time constant and specific form of configurational functions. The proposed model is applicable in a wide range of systems, providing

accurate fittings where a saturation current (i_{c0}) is observed at high voltages, such as in Fig. 4. These systems gradually increase their current with the applied voltage with a representative non-ohmic response. The actual saturation current values depend on the conditioning steps applied to the sample (i.e., voltammetry cycles), and multiple current states may be reached that are useful for analog computing systems.[5,9,18,24,54] This saturation current is not to be confused with the compliance current that is typically programmed during the measurement to avoid the damage of the sample.

As mentioned before, other resistive switching systems instead present a sudden jump to a low *resistance* state with ohmic characteristic at high voltages.[12,13] They are useful as volatile memories and only show two states of current, the highly resistive state during the sweep in the forward direction of the I–V curve and the low resistive state in the backward direction. The second type of systems will not be fitted adequately with the proposed model.

VII. CONCLUSION

It has been previously observed that the electrical response of halide perovskite memristors shows different stages according to the stationary applied potential. It evolves from a totally capacitive response at low applied voltage to a dominant inductive feature at the onset of the low resistance state. The latter feature causes the typical inverted hysteresis feature of the memristor.[21,37,50] Here, we showed a nonlinear neuron-style memristor model that enables a simultaneous analysis of small signal ac impedance and the transient behavior after a voltage pulse. The current in the capacitive domain is a decay after an initial peak. Correspondingly, the total resistance increases to the resistance value characteristic of the stationary state of the memristor. However, when the voltage pulse is higher, it activates the inductive feature. Accordingly, after the initial capacitive increase, the current rises again and the resistance traces a peak. The chemical inductor causes an increase of the current with time that explains the positive potentiation feature in which a high conductivity is achieved in successive voltage cycles. These observations provide a new tool for the quantitative interpretation of memristive synaptic dynamics by the combination of frequency and time domain electrical measurements.

ACKNOWLEDGMENTS

This study forms part of the Advanced Materials program and was supported by MCIN with funding from the European Union Next Generation EU (Grant No. PRTR-C17. I1) and Generalitat Valenciana. This work received funding from the Universidad Rey Juan Carlos, Project No. M2993.

AUTHOR DECLARATIONS

Conflict of Interest

The authors have no conflicts to disclose.

Author Contributions

Juan Bisquert: Conceptualization (lead); Formal analysis (equal); Writing – original draft (lead). **Agustín Bou**: Formal analysis (equal). **Antonio Guerrero**: Formal analysis (equal). **Enrique Hernández-Balaguera**: Formal analysis (equal).

DATA AVAILABILITY

Data sharing is not applicable to this article as no new data were created or analyzed in this study.

REFERENCES

[1]D. V. Christensen, R. Dittmann, B. Linares-Barranco, A. Sebastian, and M. Le Gallo, "2022 roadmap on neuromorphic computing and engineering," Neuromorphic Comput. Eng. **2**, 022501 (2022).
[2]M. Di Ventra, Y. V. Pershin, and L. O. Chua, "Circuit elements with memory: Memristors, memcapacitors, and meminductors," Proc. IEEE **97**, 1717–1724 (2009).
[3]Z. Xiao and J. Huang, "Energy-efficient hybrid perovskite memristors and synaptic devices," Adv. Electron. Mater. **2**, 1600100 (2016).
[4]X. Zhang, W. Wang, Q. Liu, X. Zhao, J. Wei, R. Cao, Z. Yao, X. Zhu, F. Zhang, H. Lv, S. Long, and M. Liu, "An artificial neuron based on a threshold switching memristor," IEEE Electron Device Lett. **39**, 308–311 (2018).
[5]J.-Q. Yang, R. Wang, Z.-P. Wang, Q.-Y. Ma, J.-Y. Mao, Y. Ren, X. Yang, Y. Zhou, and S.-T. Han, "Leaky integrate-and-fire neurons based on perovskite memristor for spiking neural networks," Nano Energy **74**, 104828 (2020).
[6]Y. Fang, S. Zhai, L. Chu, and J. Zhong, "Advances in halide perovskite memristor from lead-based to lead-free materials," ACS Appl. Mater. Interfaces **13**, 17141–17157 (2021).
[7]R. A. John, N. Shah, S. K. Vishwanath, S. E. Ng, B. Febriansyah, M. Jagadeeswararao, C.-H. Chang, A. Basu, and N. Mathews, "Halide perovskite memristors as flexible and reconfigurable physical unclonable functions," Nat. Commun. **12**, 3681 (2021).
[8]K. Sun, J. Chen, and X. Yan, "The future of memristors: Materials engineering and neural networks," Adv. Funct. Mater. **31**, 2006773 (2021).
[9]S. Liu, J. Guan, L. Yin, L. Zhou, J. Huang, Y. Mu, S. Han, X. Pi, G. Liu, P. Gao, and S. Zhou, "Solution-processed synaptic memristors based on halide perovskite nanocrystals," J. Phys. Chem. Lett. **13**, 10994–11000 (2022).
[10]R. Kozma, R. E. Pino, and G. E. Pazienza, *Advances in Neuromorphic Memristor Science and Applications* (Springer, 2012).
[11]Y. V. Pershin and M. Di Ventra, "Memory effects in complex materials and nanoscale systems," Adv. Phys. **60**, 145–227 (2011).
[12]R. Waser and M. Aono, "Nanoionics-based resistive switching memories," Nat. Mater. **6**, 833–840 (2007).
[13]L. Chua, "Resistance switching memories are memristors," Appl. Phys. A **102**, 765–783 (2011).
[14]B. Linares-Barranco and T. Serrano-Gotarredona, "Memristance can explain spike-time-dependent-plasticity in neural synapses," Nature Precedings (published online) (2009).
[15]S. H. Jo, T. Chang, I. Ebong, B. B. Bhadviya, P. Mazumder, and W. Lu, "Nanoscale memristor device as synapse in neuromorphic systems," Nano Lett. **10**, 1297–1301 (2010).
[16]M. Prezioso, M. R. Mahmoodi, F. M. Bayat, H. Nili, H. Kim, A. Vincent, and D. B. Strukov, "Spike-timing-dependent plasticity learning of coincidence detection with passively integrated memristive circuits," Nat. Commun. **9**, 5311 (2018).
[17]C. Wang, Z. Si, X. Jiang, A. Malik, Y. Pan, S. Stathopoulos, A. Serb, S. Wang, T. Prodromakis, and C. Papavassiliou, "Multi-state memristors and their applications: An overview," IEEE J. Emerging Sel. Top. Circuits Syst. **12**, 723–734 (2022).
[18]T. Chang, S.-H. Jo, K.-H. Kim, P. Sheridan, S. Gaba, and W. Lu, "Synaptic behaviors and modeling of a metal oxide memristive device," Appl. Phys. A **102**, 857–863 (2011).
[19]J. Bisquert and A. Guerrero, "Chemical inductor," J. Am. Chem. Soc. **144**, 5996–6009 (2022).
[20]E. Hernández-Balaguera and J. Bisquert, "Negative transient spikes in halide perovskites," ACS Energy Lett. **7**, 2602–2610 (2022).

[21] M. Berruet, J. C. Pérez-Martínez, B. Romero, C. Gonzales, A. M. Al-Mayouf, A. Guerrero, and J. Bisquert, "Physical model for the current–voltage hysteresis and impedance of halide perovskite memristors," ACS Energy Lett. **7**, 1214–1222 (2022).
[22] J. Bisquert and A. Guerrero, "Dynamic instability and time domain response of a model halide perovskite memristor for artificial neurons," J. Phys. Chem. Lett. **13**, 3789–3795 (2022).
[23] J. Bisquert, "Electrical charge coupling dominates the hysteresis effect of halide perovskite devices," J. Phys. Chem. Lett. **14**, 1014 (2023).
[24] L. Chen, C. Li, T. Huang, Y. Chen, S. Wen, and J. Qi, "A synapse memristor model with forgetting effect," Phys. Lett. A **377**, 3260–3265 (2013).
[25] C. Gonzales and A. Guerrero, "Mechanistic and kinetic analysis of perovskite memristors with buffer layers: The case of a two-step set process," J. Phys. Chem. Lett. **14**, 1395–1402 (2023).
[26] A. Solanki, A. Guerrero, Q. Zhang, J. Bisquert, and T. C. Sum, "Interfacial mechanism for efficient resistive switching in Ruddlesden-Popper perovskites for non-volatile memories," J. Phys. Chem. Lett. **11**, 463–470 (2020).
[27] J. J. Yang, D. B. Strukov, and D. R. Stewart, "Memristive devices for computing," Nat. Nanotechnol. **8**, 13–24 (2013).
[28] J. Bisquert, A. Guerrero, and C. Gonzales, "Theory of hysteresis in halide perovskites by integration of the equivalent circuit," ACS Phys. Chem. Au **1**, 25–44 (2021).
[29] A. Guerrero, J. Bisquert, and G. Garcia-Belmonte, "Impedance spectroscopy of metal halide perovskite solar cells from the perspective of equivalent circuits," Chem. Rev. **121**, 14430–14484 (2021).
[30] M. Taukeer Khan, F. Khan, A. Al-Ahmed, S. Ahmad, and F. Al-Sulaiman, "Evaluating the capacitive response in metal halide perovskite solar cells," Chem. Rec. **22**, e202100330 (2022).
[31] A. Pockett and M. J. Carnie, "Ionic influences on recombination in perovskite solar cells," ACS Energy Lett. **2**, 1683–1689 (2017).
[32] C. Gonzales, A. Guerrero, and J. Bisquert, "Transition from capacitive to inductive hysteresis: A neuron-style model to correlate I–V curves to impedances of metal halide perovskites," J. Phys. Chem. C **126**, 13560–13578 (2022).
[33] H. Bao, C. Chen, Y. Cao, S. Chang, S. Wang, and H. Zhong, "Quantitative determination of charge accumulation and recombination in operational quantum dots light emitting diodes via time-resolved electroluminescence spectroscopy," J. Phys. Chem. Lett. **14**, 1777–1783 (2023).
[34] E. Hernández-Balaguera, L. Munoz-Diaz, A. Bou, B. Romero, B. Ilyassov, A. Guerrero, and J. Bisquert, "Long-term potentiation mechanism of biological postsynaptic activity in neuro-inspired halide perovskite memristors," Neuromorphic Comput. Eng. **3**, 024005 (2023).
[35] N. Filipoiu, A. Teodora Preda, D.-V. Anghel, R. Patru, R. Elizabeth Brophy, M. Kateb, C. Besleaga, A. Gabriel Tomulescu, I. Pintilie, A. Manolescu, and G. Alexandru Nemnes, "Capacitive and inductive effects in perovskite solar cells: The different roles of ionic current and ionic charge accumulation," Phys. Rev. Appl. **18**, 064087 (2022).
[36] V. Lopez-Richard, R. S. Wengenroth Silva, O. Lipan, and F. Hartmann, "Tuning the conductance topology in solids," J. Appl. Phys. **133**, 134901 (2023).
[37] L. Munoz-Diaz, A. J. Rosa, A. Bou, R. S. Sánchez, B. Romero, R. A. John, M. V. Kovalenko, A. Guerrero, and J. Bisquert, "Inductive and capacitive hysteresis of halide perovskite solar cells and memristors under illumination," Front. Energy Res. **10**, 914115 (2022).
[38] W. Z. Shen and A. G. U. Perera, "Effect of interface states on negative capacitance characteristics in GaAs homojunction far-infrared detectors," Appl. Phys. A **72**, 107–111 (2001).
[39] J. Werner, A. F. J. Levi, R. T. Tung, M. Anzlowar, and M. Pinto, "Origin of the excess capacitance at intimate Schottky contacts," Phys. Rev. Lett. **60**, 53 (1988).
[40] X. Wu, E. S. Yang, and H. L. Evans, "Negative capacitance at metal-semiconductor contacts," J. Appl. Phys. **68**, 2845 (1990).
[41] E. Ehrenfreund, C. Lungenschmied, G. Dennler, H. Neugebauer, and N. S. Sariciftci, "Negative capacitance in organic semiconductor devices: Bipolar injection and charge recombination mechanism," Appl. Phys. Lett. **91**, 012112 (2007).
[42] J. Ding, W. Gao, L. Gao, K. Lu, Y. Liu, J.-L. Sun, and Q. Yan, "Unravelling the effect of halogen ion substitution on the noise of perovskite single crystal photodetector," J. Phys. Chem. Lett. **13**, 7831–7837 (2022).
[43] A. Podborska, M. Suchecki, K. Mech, M. Marzec, K. Pilarczyk, and K. Szaciłowski, "Light intensity-induced photocurrent switching effect," Nat. Commun. **11**, 854 (2020).
[44] W. Xu, H. Cho, Y.-H. Kim, Y.-T. Kim, C. Wolf, C.-G. Park, and T.-W. Lee, "Organometal halide perovskite artificial synapses," Adv. Mater. **28**, 5916–5922 (2016).
[45] X. Yang, Z. Xiong, Y. Chen, Y. Ren, L. Zhou, H. Li, Y. Zhou, F. Pan, and S.-T. Han, "A self-powered artificial retina perception system for image preprocessing based on photovoltaic devices and memristive arrays," Nano Energy **78**, 105246 (2020).
[46] J. Gong, H. Wei, Y. Ni, S. Zhang, Y. Du, and W. Xu, "Methylammonium halide-doped perovskite artificial synapse for light-assisted environmental perception and learning," Mater. Today Phys. **21**, 100540 (2021).
[47] S. Ham, S. Choi, H. Cho, S.-I. Na, and G. Wang, "Photonic organolead halide perovskite artificial synapse capable of accelerated learning at low power inspired by dopamine-facilitated synaptic activity," Adv. Funct. Mater. **29**, 1806646 (2019).
[48] J. Lao, W. Xu, C. Jiang, N. Zhong, B. Tian, H. Lin, C. Luo, J. Travas-sejdic, H. Peng, and C.-G. Duan, "An air-stable artificial synapse based on a lead-free double perovskite $Cs_2AgBiBr_6$ film for neuromorphic computing," J. Mater. Chem. C **9**, 5706–5712 (2021).
[49] N. Ilyas, D. Li, C. Li, X. Jiang, Y. Jiang, and W. Li, "Analog switching and artificial synaptic behavior of Ag/SiO_x:$Ag/TiO_x/p^{++}$-Si memristor device," Nanoscale Res. Lett. **15**, 30 (2020).
[50] C. Gonzales, A. Guerrero, and J. Bisquert, "Spectral properties of the dynamic state transition in metal halide perovskite-based memristor exhibiting negative capacitance," Appl. Phys. Lett. **118**, 073501 (2021).
[51] L. O. Chua and K. Sung Mo Kang, "Memristive devices and systems," Proc. IEEE **64**, 209–223 (1976).
[52] J. Bisquert, "Negative inductor effects in nonlinear two-dimensional systems. Oscillatory neurons and memristors," Chem. Phys. Rev. **3**, 041305 (2022).
[53] J. Bisquert, "Hopf bifurcations in electrochemical, neuronal, and semiconductor systems analysis by impedance spectroscopy," Appl. Phys. Rev. **9**, 011318 (2022).
[54] S. Kvatinsky, E. G. Friedman, A. Kolodny, and U. C. Weiser, "TEAM: ThrEshold adaptive memristor model," IEEE Trans. Circuits Syst. I **60**, 211–221 (2013).